Energy Advances

ROYAL SOCIETY OF CHEMISTRY

PAPER

View Article Online
View Journal | View Issue

Cite this: *Energy Adv.*, 2023, **2**, 1872

Semi-solid electrodes based on injectable hydrogel electrolytes for shape-conformable batteries†

Mario Borlaf, ‡[ab] Matias L. Picchio,[cd] Gisela Carina Luque,[c] Miryam Criado-Gonzalez, [d] Gregorio Guzmán-Gonzalez, [d] Daniel Pérez-Antolin,[ab] Gabriele Lingua,[d] David Mecerreyes *[de] and Edgar Ventosa *[ab]

The development of new battery concepts, chemistries and fabrication processes is driven by the bloom of emerging applications in a variety of fields ranging from the Internet of Things to Smart Healthcare. Shape factor-free and shape-conformable power sources are highly desired for integration with complex-shape electronic devices. Herein, a new fabrication process for shape-conformable batteries is explored. Battery cells having targeted shapes are fabricated and assisted by 3D printing. Then, flowable semi-solid electrodes are used to fill in the prefabricated parts of the battery cell. The use of injectable hydrogel electrolytes enables semi-solid electrodes to possess special rheological properties as they are flowable during the fabrication process, while gelation of the electrolytes ensures their immobility during battery operation. Herein, poly(vinyl alcohol):gallic acid gels are investigated for aqueous Zn–$LiFePO_4$ batteries. After evaluation of the effect of electrode formulation on the rheological properties as well as the ionic and electronic properties, simple-shape and UBU-shape batteries were fabricated using the best formulation. The prototype achieved areal capacities above 3 mA h cm^{-2}, utilization rate between 150 and 180 mA h g^{-1} (LFP), and capacity fading of 0.2% h^{-1}. While the prototype demonstrated the feasibility of the proposed fabrication process, improvements are still required. Shrinking of gel electrolytes and parasitic electrochemical reactions associated with the battery chemistry and the operation conditions are identified as the main challenges to be addressed for improving the performance.

Received 15th July 2023,
Accepted 14th September 2023

DOI: 10.1039/d3ya00333g

rsc.li/energy-advances

1. Introduction

Batteries are called to play a critical role in the transition to a more sustainable energy system based on renewable sources for generating electricity and fossil fuel-free transportation. New battery technologies are nowadays being developed for different applications, such as Na-ion and redox flow batteries for stationary energy storage, or Li metal and all-solid-state batteries for electromobility.[1] For certain emerging applications, flexible or shape factor-free batteries are of high interest to facilitate the integration of the energy storage system into the device. New conformable-shape supercapacitors and batteries have been shown to be suitable and promising systems[2] for applications in which commercial Li-ion or nickel-metal hydride batteries cannot fulfil shape and size requirements. For instance, shape factor-free printed power sources, as opposed to their traditional rigid counterparts, allow for seamless integration with complex-shape electronic devices.[3]

Additive manufacturing appears very attractive for the fabrication of shape-conformable batteries. Unfortunately, while 3D printing battery technology allows for fabricating such complex structures, current approaches face several important limitations.[4] Instead of addressing each of the 5 challenges individually, Borlaf *et al.*[5] proposed an innovative fabrication concept for shape-conformable batteries (injectable batteries) that combines additive manufacturing and semi-solid electrode technologies: (1) a battery cell is fabricated with the assistance of a stereolithography (SLA)-based technique leaving empty

[a] *Universidad de Burgos, Facultad de Ciencias, Dpto. Química Analítica, Plaza de Misael Bañuelos S/N, Burgos 09001, Spain. E-mail: eventosa@ubu.es*
[b] *International Research Center in Critical Raw Materials for Advanced Industrial Technologies (ICCRAM), Edificio I+D+I/CIBA, Plaza de Misael Bañuelos S/N, Burgos 09001, Spain*
[c] *Instituto de Desarrollo Tecnológico para la Industria Química (INTEC), CONICET, Güemes 3450, Santa Fe 3000, Argentina*
[d] *POLYMAT University of the Basque Country UPV/EHU, Joxe Mari Korta Center, Avda. Tolosa 72, Donostia-San Sebastián 20018, Spain. E-mail: david.mecerreyes@ehu.es*
[e] *Ikerbasque, Basque Foundation for Science, Bilbao 48013, Spain*

† Electronic supplementary information (ESI) available. See DOI: https://doi.org/10.1039/d3ya00333g

‡ Present address: Universidad Autónoma de Madrid, Department of Inorganic Chemistry, Francisco Tomás y Valiente 7, 28049 Madrid, Spain.

cavities for the electrodes and (2) semi-solid electrodes are injected into the cavities of the battery cell. Injectable semi-solid electrodes not only fill the predefined shape of the cell, but also they can be easily recycled as demonstrated in a recent work.[6] The electrochemical properties of semi-solid electrodes determine the performance of the resulting battery. In turn, the rheological properties of such semi-solid electrodes are not only essential for the fabrication process, but also for their electrochemical properties because semi-flowable semi-solid electrodes[5–9] that exhibit shear thinning and thixotropic behaviours with extremely high viscosity (paste-like slurries) are required to achieve high performances.[5] This fact leads to an apparent intrinsic limitation for semi-solid electrodes: achieving great electrochemical properties requires the semi-solid electrodes to possess rheological properties that hinder the injection process. In this context, gel-based semi-solid electrodes are great candidates to change this paradigm since their rheological properties during battery fabrication and battery operation will differ: the rheological properties of the electrolyte could potentially make semi-solid electrodes more flowable during battery fabrication and more viscous and stable during battery operation.

Different gels used as electrolytes for batteries can be found in the literature, where their design blueprint is mainly based on chemical crosslinking.[10] In this context, supramolecular hydrogels are an innovative alternative offering unparalleled versatility due to their dynamic nature.[11,12] For instance, hydrogen-bonded networks can provide shear thinning, self-healing, and thermosensitive behaviour, which are key-sought specifications for semi-solid electrodes.[13] Among the current library of building blocks with hydrogen bond motifs, natural polyphenols offer a unique combination of cost-effectiveness, multifunctionality, and extraordinary binding affinity to several water-soluble polymers for orchestrating 3D-network formation. Recently, small-sized polyphenols such as gallic acid (GA), protocatechuic acid, and pyrogallol, among others, have been demonstrated to be promising for supramolecular hydrogel chemistry.[14,15] Interestingly, poly(vinyl alcohol) (PVA):GA hydrogels feature fast gelation kinetics, shear-thinning behaviour, and low gel-to-sol phase transition temperatures (70 °C), rendering them innovative options for semi-solid electrodes.[16]

In this work, PVA:GA gels are used as electrolytes for the fabrication of shape-conformable batteries. Different hydrogel-semi-solid electrodes are evaluated as potential candidates, studying their rheological and electrochemical properties. Simple and complex-shape batteries are fabricated and evaluated using these injectable supramolecular semi-solid electrodes.

2. Experimental section

Materials and reagents

In all cases, poly(vinyl alcohol) (PVA, Merck, M_w = 61 or 146 kDa) and gallic acid (GA, ≥99.0%, Merck) were used to construct the hydrogels. Aqueous solutions of $ZnCl_2$ (97%, Alfa Aesar) and LiCl (98%, Alfa Aesar) in the presence of acetic acid (glacial, Alfa Aesar) were used as electrolyte. Lithium Iron Phosphate ($LiFePO_4$, Advanced Lithium Electrochemistry) was used as the active material. Zn plate (Alfa Aesar) and expanded graphite (bipolar plate Sigracell TF6, SGL Carbon) were used as current collectors, and CELGARD 3501 (CELGARD) as a separator. The current collectors were cut with a cutting machine Silhouette Cameo 4 (Silhouette, USA). An electroconductive carbon black powder (KetjenBlack, KB, EC-600JD, Nanografi) was used as a carbon additive to enhance the electrical conductivity.

Synthesis of hydrogels

As previously reported, the supramolecular hydrogels were synthesized following a heating/cooling protocol.[16] Different hydrogel formulations were prepared, varying the GA content and PVA molecular weight.

Table 1 summarizes the three optimized formulations chosen to study in detail the properties and electrochemical behaviour of the semi-solid electrodes. These hydrogels exhibited good flowability at high temperatures, controllable gelation kinetics, and promising processability in the gel state.

First, a $[Zn^{2+}]$ = 2 M and $[Li^{+}]$ = 0.2 M solution was prepared by dissolving $ZnCl_2$ and LiCl in water. Next, PVA and GA were added and mixed at 90 °C until their complete dissolution. After that, the mixture was transferred into a 20 mL commercial syringe (B Braun Injekt), and KetjenBlack (KB) and the active material were added and dispersed with an Ultraturrax homogenizer (IKA). Once the mixture was homogeneous, semi-solid electrodes were placed at room temperature until gelation occurred. In all cases, the active material amount was 0.5 g, and the KB amount was 0.3 g for the proportions shown in Table 1.

Rheological measurements

Oscillatory rheological measurements were carried out with an AR-G2 rheometer (TA instruments) using a stainless-steel parallel plate geometry of 20 mm diameter and a gap of 1 mm. Amplitude tests were performed from 0.01 to 1000% strain at 1 Hz and 25 °C. Dynamic mechanical thermal analysis was carried out from 20 to 90 °C at 1% strain and 1 Hz. Frequency sweeps were performed from 0.01 to 10 Hz at 1% strain and 25 °C. Shear thinning properties were measured in the shear rate range from 0.01 to 10 s^{-1} at 80 °C. The processability properties were evaluated by dynamic step-strain amplitude tests by varying the strain between 1 and 1000% at 80 °C and 25 °C.

Table 1 Hydrogel composition

Gel abbreviation	PVA (g)	GA (g)	Electrolyte solution (g)	GA:PVA ratio (wt%)
G1	0.5[a]	0.125	5	25
G2	0.375[a]	0.094	5	25
G3	0.5[b]	0.150	5	30

[a] PVA M_w: 146 kDa. [b] PVA M_w: 61 kDa.

Battery fabrication and assembly

Using an Ultraviolet (UV) Liquid Cristal Display (LCD)-based stereolithography (SLA) 3D printer Photon Mono SE (Anycubic, China) and a commercial clear resin (Anycubic, China), some parts of two different batteries were fabricated.

A battery with an active area of 5×1 cm^2 was assembled for the optimization experiments. The expanded graphite was put over a 3D printed endplate, and then, a Viton gasket of 1 mm thickness leaving a cavity of 5×1 cm^2, in which the semi-solid electrode with $LiFePO_4$ and KB was deposited. When it gelled, the separator was put on it and then, another Viton gasket, in which the electrolyte (without either $LiFePO_4$ or KB) was deposited. After gelling, the Zn plate was put as the counter-electrode, finishing the battery with another endplate. Using six screws, the battery was slightly pressed to ensure contact between all the parts.

For the complex shape batteries, the half-cells as well as a framework with the shape of the University of Burgos logo (UBU) were fabricated by 3D printing. After the cleaning procedure (with 70% isopropanol solution), the expanded graphite current collector was introduced into one half-cell, and then, the semi-solid electrode that contained LFP and KB was deposited into the cavity (1 mm of thickness). In parallel, the other half cell was put on the Zn plate current collector, and the same gel composition (in terms of PVA, GA, water, and metal ions concentration) without active material or the KB was added to fill the cavity. When both hydrogels polymerised, the separator was put on one of them, and the framework was assembled on the other half-cell. After that, both half-cells were assembled. The active area was approximately 4.7 cm^2.

Electrochemical characterization

The ionic conductivity of the hydrogels was measured by electrochemical impedance spectroscopy (EIS) using a potentiostat (Autolab PGSTAT 12, Metrohm). The frequency range was set from 1×10^5 to 0.01 Hz, and the amplitude was 10 mV. The hydrogels were deposited on a separator-free cell of 2 cm diameter and 2 mm thickness, using two current collectors of expanded graphite.

The batteries were characterized by galvanostatic charge–discharge measurements by using a cycler (NEWARE, China) at a current density of 0.5 mA cm^{-2} and a voltage ranging between 0.3 and 1.55 V.

3. Results and discussion

3.1. Synthesis and characterization of carbon-containing hydrogels

The quantity of KB influences both the rheological and electrochemical properties of the semi-solid electrode. Also, other parameters such as type of carbon additive, particle size and content of active material will influence the properties of the

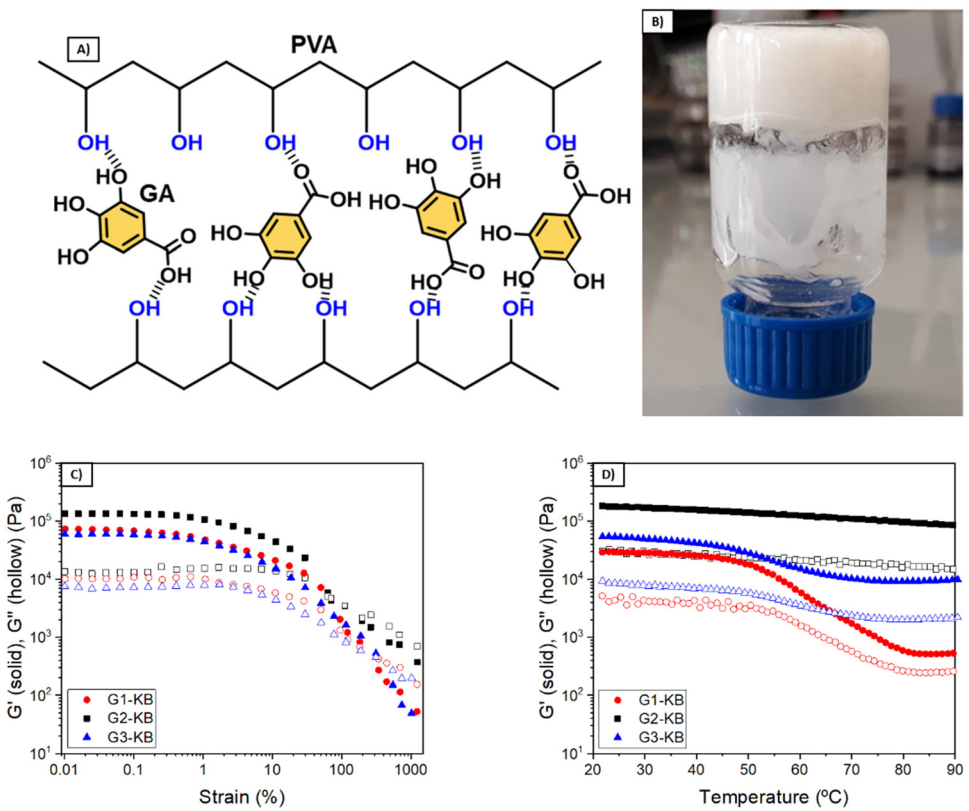

Fig. 1 (A) Schematic representation of the hydrogel formation. (B) Photograph of a PVA-GA hydrogel (without carbon). Evolution of the elastic modulus (G') and loss modulus (G'') of GX–KB gels (with carbon) with different GA percentages as a function of the strain (C) and temperature (D).

semi-solid electrode and thus the overall performance. In this work, the number of variables was fixed (particle size and content of active material and particle size), so that various formulations using different quantities of PVA and GA were investigated to focus the attention on the influence of the hydrogel electrolyte. PVA and GA show a strong binding affinity by hydrogen bonding, forming stable networks in a few minutes (Fig. 1A and B). Several formulations were evaluated to obtain tailor-made hydrogels, changing the polymer molecular weight (M_w = 61 or 146 kDa) and the PVA and GA concentrations. Fig. 1C and D show the viscoelastic properties of the three different optimized GX–KB gel formulations (the gels containing carbon black were coded as GX–KB, where X is the number associated in Table 1). At 25 °C, G2–KB exhibits a solid-like behaviour with a value of the elastic modulus (G') higher than the loss modulus (G'') up to a yield strain of 70% (Fig. 1C) when it starts to flow, exhibiting a liquid-like behaviour ($G'' > G'$). For G1-KB and G3–KB gels, an increase of the yield strain up to 320% is observed, which is associated with the higher crosslinking density between the PVA chains and GA in these samples. Dynamic mechanical thermal analysis from 20 to 90 °C was performed to study the thermal transition of the gels (Fig. 1D). As shown in Fig. S1 (ESI†), the G1 gel (where only hydrogen bonds are present) exhibits a thermal transition at 52 °C leading to the total melting of the network passing from a solid-like state to a liquid-like state. This temperature-dependent behaviour is characteristic of polymer networks formed by hydrogen bonds.[17,18] Curiously, the incorporation of KB suppresses the gel-to-sol phase transition, although G1-KB gel exhibits a substantial decrease of G' and G'' from 55 °C to 80 °C, where a new steady state is reached. This result indicates that the additive KB gives a solid-like structure to the network. The role of KB in the viscoelastic properties of the gels is more evident in the G2–KB formulation, which has a higher carbon content based on PVA of 80%, compared to 60% for G1-KB. In G2–KB, G' and G'' remain almost constant with the temperature, meaning carbon particles can act as physical crosslinking points and are predominant in the gel network.[19,20] Even if increasing the GA percentage up to 30 wt%, the G3–KB gel shows a less prominent temperature-dependence of the dynamic moduli than G1-KB,

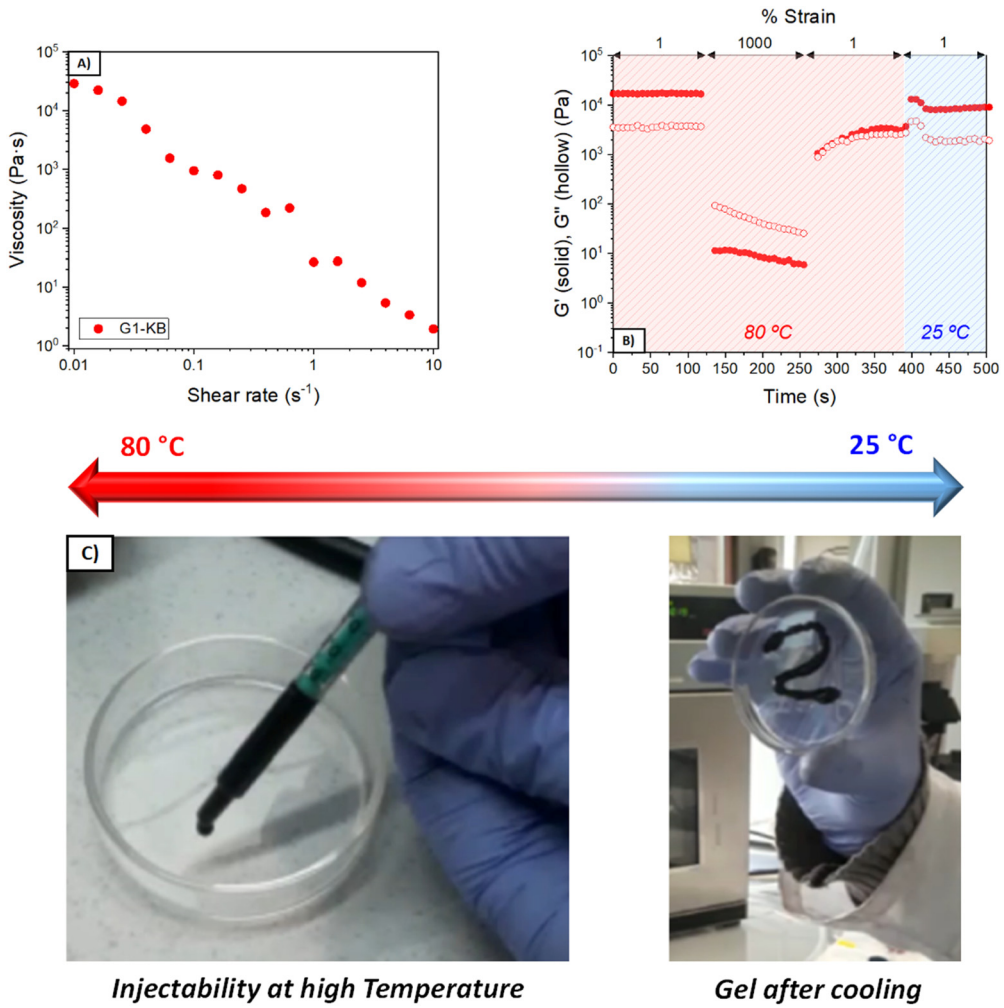

Fig. 2 (A) Shear thinning properties of G1-KB gel. (B) Dynamic step strain test of G1-KB gel to determine the injectability properties. (C) Photographs of G1-KB gel passing through a syringe at high temperature and final appearance after injection and cooling.

which suggests that the influence of carbon particles is more critical when a PVA of lower molecular weight is used (145 kDa in G1-KB *vs.* 65 kDa in G3–KB). Therefore, G1-KB gel was selected for further thermo-processability tests.

The addition of carbon additive to the hydrogel electrolyte changes significantly its properties to a point in which the hydrogel might not be formed. Since the semi-solid electrode must contain carbon additive with high surface area, further studies focused on the characterization of the carbon-containing hydrogel electrolyte (GX–KB gel). One requirement of injectable materials is to exhibit shear-thinning properties. Thus, flow tests were performed at 80 °C, and the results showed a viscosity decrease with the shear rate revealing the shear-thinning behaviour of the GX–KB gels (Fig. 2A and Fig. S2A, ESI†). Apart from that, injectable gels must possess thixotropy with a recovery of their viscoelastic properties after being subjected to a shear force.[21,22] To that aim, dynamic step-strain amplitude tests were carried out (Fig. 2B and Fig. S2B, ESI†). At low strains (1%) and a high temperature (80 °C), the GX–KB gels exhibit a solid-like behaviour ($G' > G''$). After increasing the strain up to 1000% at 80 °C, there is a drastic decrease of G' reaching a liquid-like state ($G'' > G'$). Interestingly, after removing the high strain applied, a total recovery of the initial mechanical properties and the solid-like state is observed in G1-KB ($G' > G''$), which remains constant after cooling the gels at 25 °C. However, in G2–KB and G3–KB the mechanical properties after cooling differ from the initial ones, which confirms that G1-KB is the most appropriate gel for the semi-solid electrode preparation. The injectability properties were also assessed by passing the G1-KB gel, previously heated at 80 °C, through a syringe, drawing a zig-zag curve that remains stable without sliding after cooling at 25 °C (Fig. 2C). Based on the above results regarding temperature-dependence, the proposed hydrogels also contribute to a potential recycling process. The possibility of heating up the battery above the gel–sol transition temperature (<80 °C) to make the electrolyte liquid, also facilitates the recyclability process because the used electrolyte can be ejected from the battery and then, the active materials, the carbon additive and the electrolyte can be easily separated and recovered by simple filtration and cleaning procedures. Moreover, such hydrogels can be also potentially exploited as printable electrodes using a 3D printer with a heater reservoir in which the hydrogels are kept at temperatures above the temperature transition to ensure the "liquid state". Then, the hydrogels would be extruded and deposited on a cooled platform, battery, or current collector to promote a fast gelation and create the 3D-printed hydrogel electrolyte or semi-solid electrode.

Another important parameter is the shrinkage of the hydrogel during the supramolecular assembly. Photographs of the

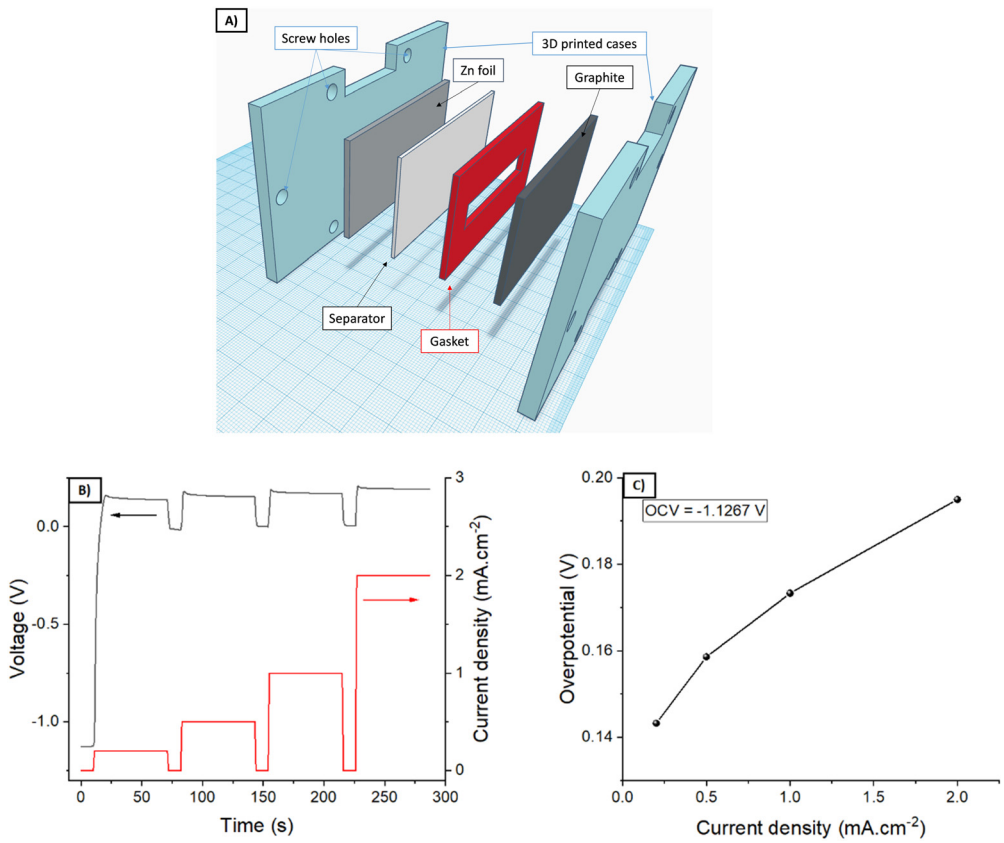

Fig. 3 (A) Scheme of the cell containing a Zn foil and expanded graphite current collectors. G1–KB was used as a case study, using 2 mm of thickness. (B) Evolution of the potential as a function of the applied current with time. (C) Overall overpotential as a function of the applied current density.

different hydrogels (without carbon) as prepared and after 24 h are shown in Fig. S3 (ESI†). Hydrogels G1 and G2 exhibited a shrinkage of approximately 2 vol%, while G3 is around 1 vol%. Although this decrease may seem neglectable, it is pointed out for further discussion in the electrochemical characterization section. Considering that G3 is formed by using a greater GA:PVA ratio and a low molecular weight PVA (61 kDa), the lower observed shrinkage is in good agreement with the expected results because the polymer chains are shorter and with fewer hydrogen bond interactions, as supported by the rheological results.

3.2. Electrochemical properties of carbon containing hydrogels

First of all, the ability of G1 hydrogel electrolyte to transport Zn ions was evaluated by placing the G1–KB gel between a Zn metal foil and an expanded graphite current collector (Fig. 3A). Upon application of an external bias, Zn is oxidized to Zn^{2+}, which diffuses to the graphite current collector to be reduced on the electrode surface. The overall overpotential results from the sum of several resistances: ionic resistance, charge transfer resistance (kinetics) for Zn stripping/plating, and concentration gradient of Zn-ions. Fig. 3B shows the voltage profile for pulses of 1 min at increasing values of current density, leaving a rest of 10 s (open circuit potential) between two pulses. The results are summarised in Fig. 3C (overpotential *versus* applied current density). While the overpotentials increased with increasing current density as expected, the overpotential values of below 200 mV obtained at 2 mA cm^{-2} indicate that the hydrogel is able to transport Zn^{2+} sufficiently fast to operate a battery using these types of hydrogels up to 2 mA cm^{-2}. It should be noted that the electrochemical determination of the transfer number for Zn in neutral pH was very unreliable due to the hydrogen evolution during Zn plating at very low current densities required for the measurement. Then, the stability window of the hydrogels was evaluated (Fig. S4, ESI†). G1, G2 and G3 showed similar behaviour indicating that they are stable between 0 V/1.55 V *vs.* Zn/Zn^{2+} (−0.34 V/1.21 V *vs.* RHE in neutral pH), which covers the potential range for the target battery chemistry (Zn–$LiFePO_4$).

Using a separator-free cell (Fig. 4A), the electronic and ionic conductivity of the G1–KB, G2–KB, and G3–KB gels were calculated from EIS measurements (Fig. 4B and Table 2).[6] It is important to stress the lack of membrane in the cell for these measurements. Intrinsic properties of carbon-containing hydrogel electrolytes are difficult to estimate in the conventional cell configuration. For instance, the electronic conductivity of the semi-solid electrode cannot be unambiguously determined when a separator is used. Therefore, the intrinsic electrochemical properties of the carbon-containing hydrogel electrolytes were evaluated in a membrane-free cell, which resembles the experimental setup used for the evaluation of mixed electric and ionic conductors in solid oxide fuel cells. Indeed, the semi-solid electrodes can be considered as a mixed ionic and electric conductor since the solid particles transport electrons and the electrolyte in the slurry provides ionic conductivity. If an electric barrier such as a separator or membrane is used in the cell, electrons cannot flow between the two current collectors through the semi-solid electrode. Thus, the separator/membrane is removed so that the cell is ''short-circuited'' and pure electric resistance through the semi-solid electrode can be measured. As the resulting setup resembles that of solid oxide fuel cells, the equivalent circuit typically used for solid oxide fuel cells is used (Fig. S5, ESI†), in which low frequencies provide the electric conductivity (similar to DC measurements). High frequencies should be dominated by the ionic conductivity, while it can be influenced by electric conductivity (current might leak through the electric resistor if the resistance is very small). The GX–KB gels behave as mixed ionic

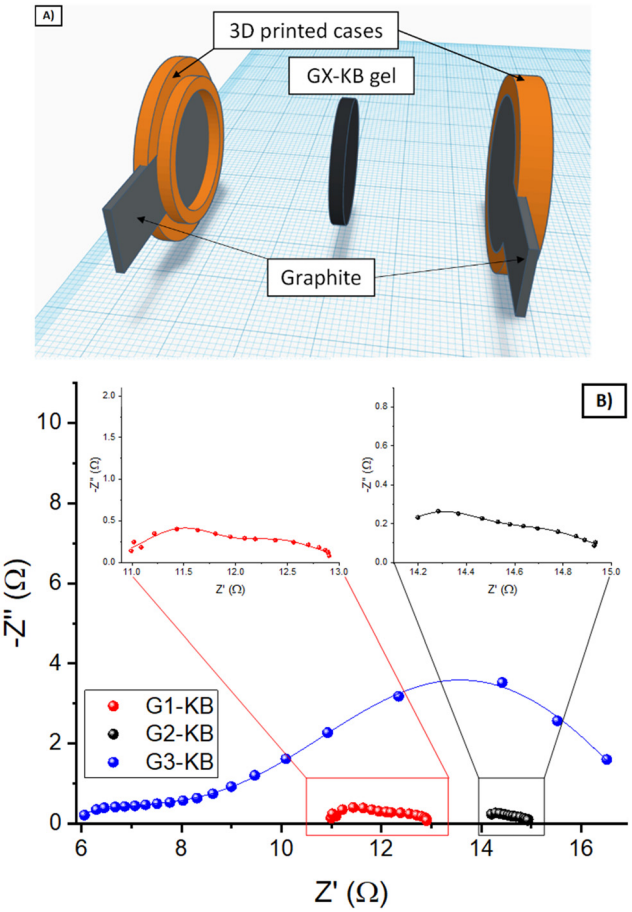

Fig. 4 (A) Scheme of the membrane-free cell with two expanded graphite current collectors and a cavity for 2 mm thickness. (B) Nyquist plots of the EIS measurements for carbon-containing gels.

Table 2 Electronic and ionic conductivity of the carbon-containing hydrogels

Gel	Electronic conductivity (S cm^{-1})	Ionic conductivity (S cm^{-1})
G1–KB	4.97×10^{-3}	4.21×10^{-4}
G2–KB	4.24×10^{-3}	1.16×10^{-4}
G3–KB	3.74×10^{-3}	4.74×10^{-3}

and electric conductors, so the equivalent circuit used was obtained from the literature of this field (Fig. S5, ESI†).[23] On the one hand, the electronic conductivities are quite similar for all cases. On the other hand, the G3–KB exhibits a greater value of ionic conductivity (one order of magnitude than the other gels). This is attributed to the shorter polymer chains with fewer hydrogen bond interactions for G3–KB, which enables higher mobility of ions. These results are also in good agreement with the shrinkage behaviour of the gels.

3.3. Batteries based on hydrogel semi-solid electrodes

Based on the results from the rheological and electrochemical characterization, G1–KB and G3–KB gels were selected for further evaluation as potential candidates for injectable batteries. After adding the active material, the semi-solid electrodes (carbon-containing gel + active material, Fig. 5A) were injected into the cavities of the battery. However, the slow gelation kinetics for G3–KB provoked sedimentation, ruling out the use of this formulation for an injectable battery. On the other hand, the faster gelation for G1–KB and the shrinkage of the gel resulted in a poorer contact between the semi-solid electrode and the different parts of the battery, leading to large overpotentials and impeding its operation. It should be noted that the injectable battery cell was not pressed after injection since the SLA-printed cell was not compressible. Thus, the cavities conformed by the SLA printing were filled with the G1–KB semi-solid electrode before assembling to overcome the shrinking issue from an engineering approach. It should be noted that the shrinkage issues are currently being addressed from a chemical approach by designing non-shrinkable hydrogel-based semi-solid electrodes. Further optimization by varying the particle size and content of active material and carbon additive will be carried out when a more suitable hydrogel electrolyte is found.

A simple-shape battery ($L \times W \times H = 5 \times 1 \times 0.1$ cm^3) containing a Zn|G1‖G1–KB+LFP|graphite (Fig. 5B) was fabricated using gaskets as a starting point. Fig. 5C and D show the voltage profiles and the evolution of the charge capacity (and coulombic efficiency) with the number of cycles during 336 h of operation. The voltage profile reveals an overpotential of *ca.* 300 mV and the typical shape for a Zn-LFP battery when operated at 0.5 mA cm^{-2}. The larger overpotentials compared with other aqueous Zn-LFP cells reported in the literature are associated with the use of thick electrodes (1 mm thick) and hydrogel electrolytes.[24] The specific capacity in the first cycle was estimated to be 184 mA h g^{-1}, which confirms a high utilization rate. As a matter of fact, the areal capacity, which is an important practical parameter, is significantly larger than those achieved in previous studies.[24] While the battery cell was able to store energy reversibly, the coulombic efficiency in the first cycles remained at 92–95%, probably due to the parasitic reactions at the negative electrode during the charging process.

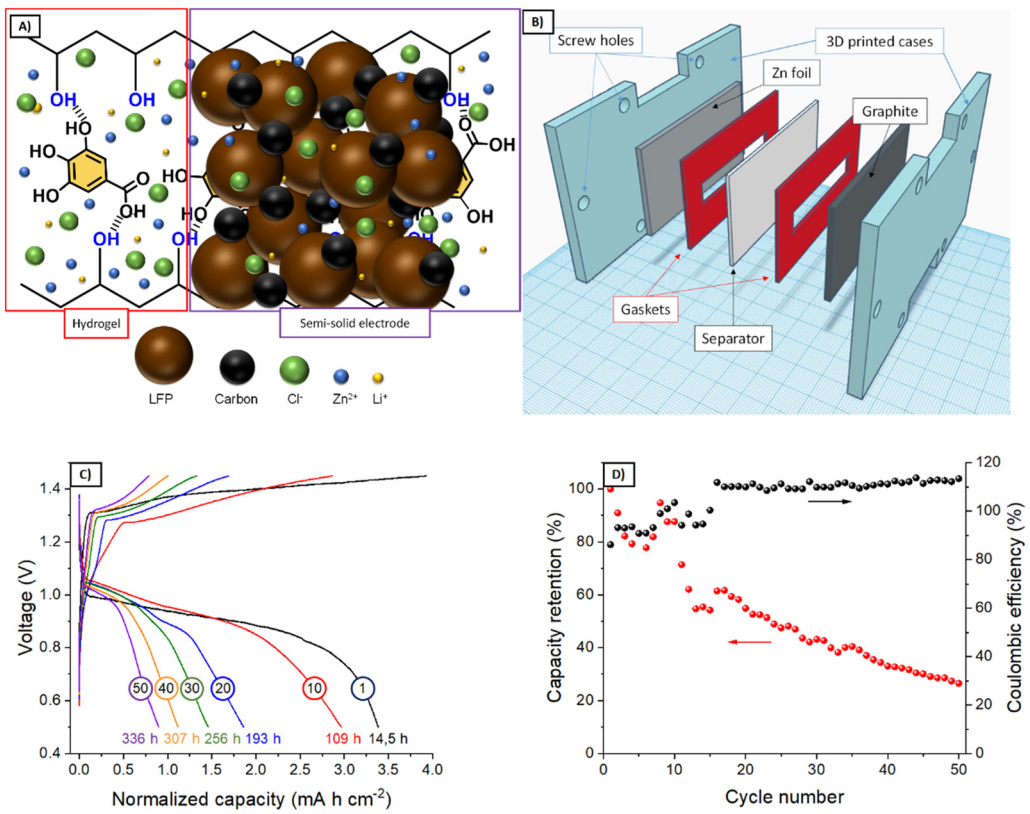

Fig. 5 (A) Scheme of the semi-solid electrode composition. (B) Schematic representation of the simple-shape battery. (C) Voltage profiles for the Zn|G1‖G1–KB+LFP|graphite simple-shape battery ($L \times W \times H = 5 \times 1 \times 0.1$ cm^3) operated at 0.5 mA cm^{-2}. A specific capacity of 184 mA h g^{-1} was obtained for the 1st cycle. (D) Evolution of the charge capacity and coulombic efficiency with the number of cycles. Total cycling time was 336 h.

Indeed, coulombic efficiencies above 100% after 20 cycles indicate that capacity decay is promoted during the charging process. All this led to an accelerated capacity decay of *ca.* 70% in 50 cycles per 336 h (Fig. 5C), resulting in a capacity fading of 0.2% h^{-1}. While the results demonstrate the feasibility of using hydrogel-based semi-solid electrodes for the proposed fabrication procedure, several strategies for improving the electrochemical performance are currently being pursued: other families of hydrogel electrolytes with improved characteristics, the decrease in areal capacity, *i.e.*, thinner electrodes (related to more suitable rheological properties) for improving the coulombic efficiency, and the implementation of other

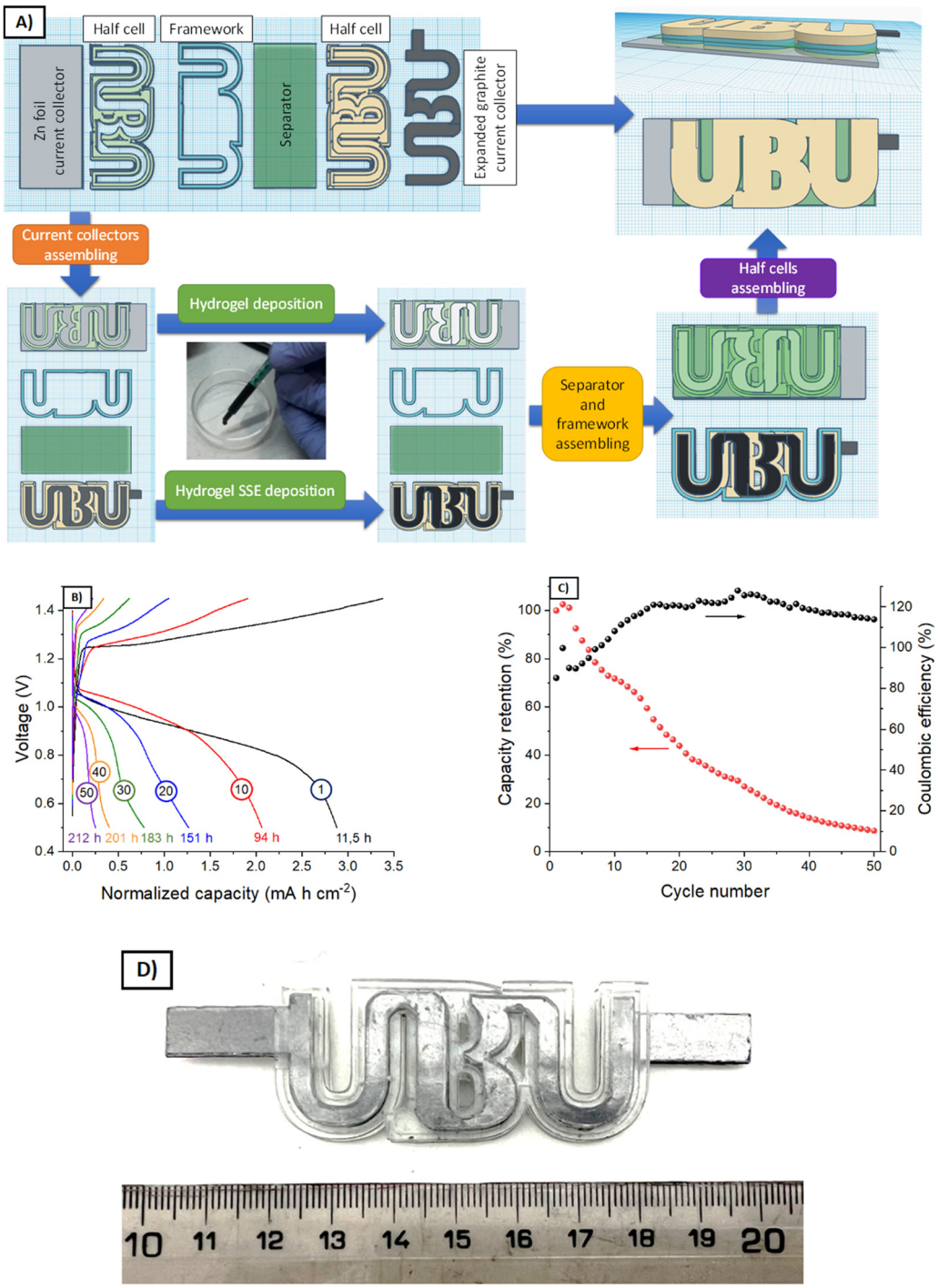

Fig. 6 (A) Scheme of the UBU-shape full battery assembling process. SSE means semi-solid electrode. (B) Voltage profiles for the Zn|G1‖G1–KB+LFP|graphite UBU-shape battery (4.7 cm^2 × 0.1 cm thickness) operated at 0.53 mA cm^{-2}. A specific capacity of 147 mA h g^{-1} was obtained for the 1st cycle. (C) Evolution of charge capacity and coulombic efficiency with the number of cycles. Total cycling time was 212 h. (D) Photograph of a UBU-shape prototype.

active materials. In this sense, the proposed approach will also benefit from any improvements achieved in the field of conventional batteries, such as new current collectors preventing parasitic reaction for neutral pH.

After evaluating the semi-solid electrodes in a simple-shape cell, the final goal is to use them in shape-conformable batteries of complex geometries. Thus, an UBU-shape cell was fabricated following the procedure described in Fig. 6A (see a photograph of a prototype in Fig. 6D) and evaluated. Fig. 6B and C shows the voltage profiles and the evaluation of the charge capacity (and coulombic efficiency) with the number of cycles (and time). While few differences were noted for simple and complex-shape batteries (specific capacity of 184 and 147 mA h g^{-1} for simple and complex shape, respectively), the overall performances were similar. Regarding the voltage profiles, the UBU-shape delivered lower overpotentials at the beginning of the charge/discharge process, while a sloppier evolution of the voltage upon the (dis-)charge process was observed with respect to the simple geometry. From the voltage profiles, it could be expected that the cycling stability would improve for the complex-shape battery, but it did not. Actually, the capacity retention decreased. These two facts indicate that the homogeneity of the distribution of active material in the UBU-shape batteries worsened with respect to the simple-shape battery. It should be noted that semi-solid electrodes were spread manually, and complex shapes will benefit from the automatization of this process. In any case, Fig. 6 shows the feasibility of using hydrogel-based semi-solid electrodes for shape-conformable batteries of complex geometries.

4. Conclusions

In this work, hydrogel electrolytes based on PVA:GA were investigated and employed to prepare semi-solid electrodes for shape-conformable batteries. The results showed that carbon-containing hydrogels exhibited shear thinning behaviour, a prominent thermal transition, good electrical and ionic conductivities, and enough Zn transport. In particular, the formulation containing 0.5 g PVA (M_w = 146 kDa), 0.125 g gallic acid, 5 g electrolyte solution, 1 g $LiFePO_4$ (14.4 wt% $LiFePO_4$ as active material) and 0.3 g carbon additive was employed as an injectable electrode material for the fabrication of simple rectangular-shape and UBU-shape full batteries. The electrochemical performances of both simple- and complex-shape batteries were similar. Areal capacities above 3 mA h cm^{-2} and utilization rates between 150 and 180 mA h g^{-1} (LFP), approximately, were achieved. While the cycling stability certainly required further investigation to prevent the occurrence of parasitic reactions (other electrolytes, active materials, and thinner electrodes) and improve the capacity fading of 0.2% h^{-1}, the prototypes fabricated in this work demonstrated the feasibility of using hydrogel-based semi-solid electrodes for shape-conformable batteries.

Conflicts of interest

There are no conflicts to declare.

Acknowledgements

The authors acknowledge the financial support by the Spanish Ministry of Science and Innovation and NextGenerationEU (TED2021-131651B-C21 and TED2021-131651B-C22) and Ramón y Cajal award (Ministry of Science and Innovation and European Social Funds, RYC2018-026086-I). This work was supported by the Regional Government of Castilla y León (Junta de Castilla y León) and by the Ministry of Science and Innovation MICIN and the European Union NextGenerationEU/PRTR (C17. I1). The Marie Sklodowska-Curie Research and Innovation Staff Exchanges (RISE) support under the grant agreement No 823989 ''IONBIKE'' is also greatly acknowledged.

References

1 N. Nitta, F. Wu, J. T. Lee and G. Yushin, *Mater. Today*, 2015, **18**, 252–264.
2 Y. Khan, A. E. Ostfeld, C. M. Lochner, A. Pierre and A. C. Arias, *Adv. Mater.*, 2016, **28**, 4373–4395.
3 D. B. Ahn, S. S. Lee, K. H. Lee, J. H. Kim, J. W. Lee and S. Y. Lee, *Energy Storage Mater.*, 2020, **29**, 92–112.
4 Y. Pang, Y. Cao, Y. Chu, M. Liu, K. Snyder, D. MacKenzie and C. Cao, *Adv. Funct. Mater.*, 2020, **30**, 1906244.
5 M. Borlaf, R. Moreno and E. Ventosa, *J. Power Sources*, 2023, **570**, 233063.
6 D. Perez-Antolin, R. Trócoli, J. Palma and E. Ventosa, *J. Power Sources*, 2020, **480**, 228839.
7 D. Perez-Antolin, I. Sáez-Bernal, A. Colina and E. Ventosa, *Electrochem. Commun.*, 2022, **138**, 107271.
8 D. Perez-Antolin, C. Irastorza, S. Gonzalez, R. Moreno, E. García-Quismondo, J. Palma, J. J. Lado and E. Ventosa, *Desalination*, 2022, **533**, 115764.
9 D. Perez-Antolin, W. Schuhmann, J. Palma and E. Ventosa, *J. Power Sources*, 2022, **536**, 231480.
10 Y. Guo, J. Bae, F. Zhao and G. Yu, *Trends Chem.*, 2019, **1**, 335–348.
11 K. Kurihara, *Encyclopedia of Polymeric Nanomaterials*, 2015, pp. 2372–2377.
12 E. A. Appel, J. del Barrio, X. J. Loh and O. A. Scherman, *Chem. Soc. Rev.*, 2012, **41**, 6195–6214.
13 G. Zhang, Y. Chen, Y. Deng, T. Ngai and C. Wang, *ACS Macro Lett.*, 2017, **6**, 641–646.
14 J. C. Bonafé Allende, R. N. Schmarsow, E. Matxinandiarena, S. D. García Schejtman, E. A. Coronado, C. I. Alvarezigarzabal, M. L. Picchio and A. J. Müller, *Macromolecules*, 2022, **55**, 10870–10879.
15 E. M. Euti, A. Wolfel, M. L. Picchio, M. R. Romero, M. Martinelli, R. J. Minari and C. I. A. Igarzabal, *Macromol. Rapid Commun.*, 2019, **40**, 1900217.
16 A. Wolfel, E. M. Euti, M. L. Picchio, M. R. Romero, V. M. Galvan Josa, M. Martinelli, R. J. Minari and C. I. Alvarez Igarzabal, *Polym. Chem.*, 2020, **11**, 7185–7198.
17 G. C. Luque, M. L. Picchio, A. P. S. Martins, A. Dominguez-Alfaro, N. Ramos, I. del Agua, B. Marchiori, D. Mecerreyes,

R. J. Minari and L. C. Tomé, *Adv. Electron. Mater.*, 2021, **2100178**, 2100178.
18 A. Choperena and P. Painter, *Macromolecules*, 2009, **42**, 6159–6165.
19 M. Criado-Gonzalez, D. Wagner, J. Rodon Fores, C. Blanck, M. Schmutz, A. Chaumont, M. Rabineau, J. B. Schlenoff, G. Fleith, J. Combet, P. Schaaf, L. Jierry and F. Boulmedais, *Chem. Mater.*, 2020, **32**, 1946–1956.
20 S. Khodabakhshi, P. F. Fulvio and E. Andreoli, *Carbon*, 2020, **162**, 604–649.
21 A. Lejardi, R. Hernández, M. Criado, J. I. Santos, A. Etxeberria, J. R. Sarasua and C. Mijangos, *Carbohydr. Polym.*, 2014, **103**, 267–273.
22 M. Criado-Gonzalez, E. Espinosa-Cano, L. Rojo, F. Boulmedais, M. R. Aguilar and R. Hernández, *ACS Appl. Mater. Interfaces*, 2022, **14**, 10068–10080.
23 R. A. Huggins, *Ionics*, 2002, **8**, 300–313.
24 N. Yesibolati, N. Umirov, A. Koishybay, M. Omarova, I. Kurmanbayeva, Y. Zhang, Y. Zhao and Z. Bakenov, *Electrochim. Acta*, 2015, **152**, 505–511.